Molecular bases of cyclodextrin adapter interactions with engineered protein nanopores

Arijit Banerjee[a], Ellina Mikhailova[a], Stephen Cheley[a], Li-Qun Gu[b,2], Michelle Montoya[c,3], Yasuo Nagaoka[a,4], Eric Gouaux[d], and Hagan Bayley[a,1]

[a]Department of Chemistry, University of Oxford, Oxford, OX1 3TA, United Kingdom; [b]Department of Medical Biochemistry & Genetics, Texas A&M University System Health Science Center, College Station, TX 77843-1114; [c]Department of Biochemistry and Molecular Biophysics and Howard Hughes Medical Institute, Columbia University, New York, NY 10032; and [d]Vollum Institute and Howard Hughes Medical Institute, Oregon Health and Science University, Portland, OR 97239

Engineered protein pores have several potential applications in biotechnology: as sensor elements in stochastic detection and ultrarapid DNA sequencing, as nanoreactors to observe single-molecule chemistry, and in the construction of nano- and micro-devices. One important class of pores contains molecular adapters, which provide internal binding sites for small molecules. Mutants of the α-hemolysin (αHL) pore that bind the adapter β-cyclodextrin (βCD) ~10^4 times more tightly than the wild type have been obtained. We now use single-channel electrical recording, protein engineering including unnatural amino acid mutagenesis, and high-resolution x-ray crystallography to provide definitive structural information on these engineered protein nanopores in unparalleled detail.

alpha-hemolysin | single molecule | stochastic sensing | structure | unnatural amino acid

Many research groups have used protein engineering to obtain enzymes and antibodies with new properties suited for specific tasks (1–6). Fewer groups have taken on the difficult problem of engineering membrane proteins (7). We have engineered the α-hemolysin protein pore, mindful of several potential applications in biotechnology, including its ability to act as a detector in stochastic sensing (8) and ultrarapid DNA sequencing (9), to serve as a nanoreactor for the observation of single-molecule chemistry (10) and to act as a component for the construction of nano- and microdevices (11).

An important breakthrough in this area, which enabled the stochastic sensing of organic molecules including the detection of DNA bases in the form of nucleoside monophosphates (12, 13), was the discovery of internal molecular adapters, a form of noncovalent protein modification (14). Most useful have been cyclodextrin (CD) adapters, which have until now been used in the absence of detailed structural information about how they work. The present paper is a definitive investigation, which provides such information through the application of a wide variety of technical approaches: single-channel electrical recording, protein engineering including unnatural amino acid mutagenesis, and x-ray crystallography. The studies employing mutagenesis show that the striking interactions seen in the crystal structures also occur in individual pores in lipid bilayers.

We reveal that the tight-binding αHL mutants (15) M113N$_7$ and M113F$_7$ bind βCD in different orientations within the heptameric pore. In the case of M113N$_7$, the top (primary hydroxyls) of the CD ring faces the trans entrance of the pore. In the case of M113F$_7$, the bottom (secondary hydroxyls) of the CD ring faces the trans entrance, while the top of the ring is bonded to the pore through remarkable CH-π interactions. Another tight-binding mutant, M113V$_7$, can bind the CD in both orientations. These results illustrate the exquisite level of engineering that can be achieved with protein nanopores, which is, for example, far beyond what is possible with solid-state pores. The work also provides information valuable for the design of new binding sites

within the lumen of the αHL pore or within other β-barrel proteins. Our results will be of interest to others exploring the interactions of CDs with the αHL pore (16, 17), including groups involved in computational studies (18, 19). In addition CDs bind to a variety of other pores, including porins (20, 21) and connexins (22), and are being tested in vivo as blockers of the anthrax protective antigen pore (23, 24). The CD adapter concept has also been incorporated into other formats, e.g., with glass nanopores (25), and artificial pores based on CDs have been made by several groups (26–28). Our work is pertinent to these studies.

Results

Kinetics and Thermodynamics of the Interactions of βCD with αHL Pores Containing Met, Phe and Asn at Position 113. We showed earlier that position 113 in the αHL pore (Fig. 1A) is critical for the binding of βCD (14). Subsequently, residue 113, which is Met in the WT protein, was changed to each of the remaining 19 naturally occurring amino acids by site-directed mutagenesis (15). We found that 11 of these mutants, expressed as homoheptamers, bound βCD with a similar affinity and with similar kinetics to the WT homoheptamer. Two mutants (P, W) bound βCD about 10 times more strongly than the WT homoheptamer, while six of them (V, H, Y, D, N, F) bound with high affinity, i.e., with a K$_d$ value 10^3 to 10^4 times lower than the WT.

Remarkably, the side chains of the latter six amino acids bear little resemblance to one another, and this issue is addressed in the present paper. We first examined the two amino acids with the most disparate side chains (F and N) by making heteromeric pores containing WT (Met-113), M113F, and M113N subunits. Three series of heteroheptamers were produced: WT$_{7-n}$M113N$_n$, WT$_{7-n}$M113F$_n$, and M113F$_{7-n}$M113N$_n$. The heteroheptamers were separated by SDS-polyacrylamide gel electrophoresis aided by an oligoaspartate (D8) tail on the first of the two types of subunit (Fig. 1B) (29). All 21 combinations of WT, M113F, and M113N subunits formed αHL pores that interacted with βCD as shown by single-channel current recordings, which revealed the extent of block by βCD (Fig. S1), the association and dissociation
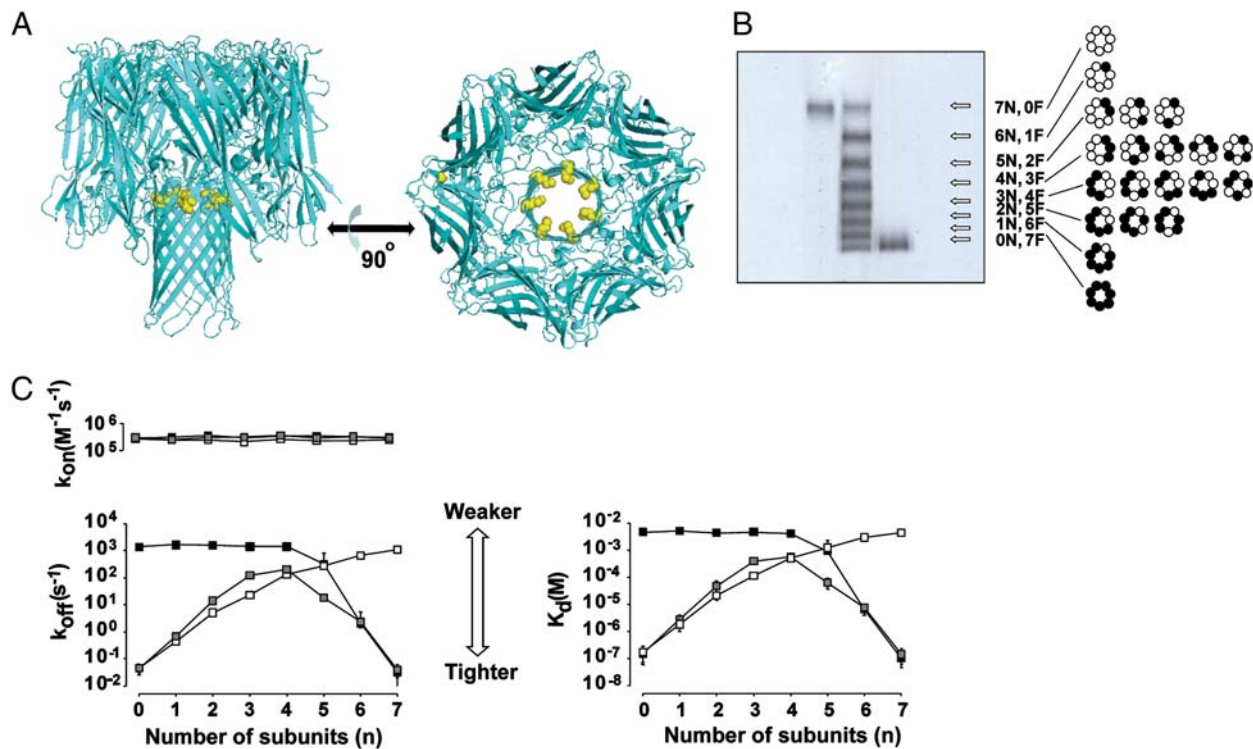
BIOCHEMISTRY

Fig. 1. Binding of βCD by heteromeric αHL pores formed by WT, M113F and M113N subunits. (*A*) Crystal structure of WT-αHL (61) showing residue 113 (Met, yellow). Left panel, side view and right panel, top view. (*B*) Separation of ^{35}S-labeled αHL heteroheptamers by SDS-polyacrylamide electrophoresis. The separation of the $M113F_{7-n}M113N_n$ heteromers is shown as detected by autoradiography of a dried gel. The M113F subunits carried a D8 tail. Lane 1, $M113N_7$; lane 2, $M113F_{7-n}M113N_n$ (the heteromers formed from several preparations made with differing ratios of M113F and M113N subunits were mixed to give roughly equal amounts of each subunit combination); lane 3, $M113F_7$. A diagram of the eight different combinations of subunits and their permutations is shown to the right of the autoradiogram. The various permutations are not separated by electrophoresis. (*C*) Kinetics of the interaction of βCD with single heteromeric αHL pores as determined by bilayer recording. Values of k_{on} were calculated by using $k_{on} = 1/(\tau_{on}[\beta CD])$, where τ_{on} is the mean interevent interval. Values of k_{off} were determined by using $k_{off} = 1/\tau_{off}$, where τ_{off} is the mean dwell time of βCD in the pore. Values of K_d were calculated by using $K_d = k_{off}/k_{on}$. Each point represents the mean ± s.d. for three or more determinations. Where they cannot be seen, the s.d. values lie within the symbol. Black squares, $WT_{7-n}M113N_n$; gray squares, $M113F_{7-n}M113N_n$; empty squares, $M113F_{7-n}WT_n$.

rate constants for βCD (k_{on} and k_{off}), and (from the latter) the equilibrium dissociation constant for βCD ($K_d = k_{off}/k_{on}$) (15).

The k_{on} values for βCD for the 21 combinations of subunits were all similar at ~5 × 10⁵ M⁻¹ s⁻¹ (Fig. 1*C, Upper*). By contrast, the k_{off} values differed widely, ranging from ~5 × 10⁻² s⁻¹ to ~10³ s⁻¹. For $WT_{7-n}M113N_n$ and $WT_{7-n}M113F_n$, the k_{off} values decreased as M113N or M113F subunits were added. In the case of M113N, there was a steep drop in the value of k_{off} after the fifth subunit had been incorporated. In the case of M113F, the decrease in the value of k_{off} occurred less precipitously as the M113F subunits were added (Fig. 1*C, Lower*). Intriguingly, with $M113F_{7-n}M113N_n$, k_{off} first increased as M113N subunits were added to $M113F_7$ until $n = 4$ ($M113F_3M113N_4$) and then decreased for larger values of n (Fig. 1*C*, Lower). We recognize that there is more than one permutation of heteromers containing two to five mutant subunits (Fig. 1*B*), but we have ignored this fact here because no significant differences in the properties of individual heteromers were observed. For example, 42 recordings were made of WT_5M113N_2, which has three permutations. Because, k_{on} showed little variation with subunit composition, the variation in K_d was similar to the variation in k_{off} (Fig. 1*C*).

While these studies were in progress, the crystal structures of βCD complexed to $M113N_7$ (Fig. 2*B*) and $M113F_7$ (Fig. 2*C*) were solved (Table S1) (30). High-resolution structures could be obtained because the CD and the αHL pore have the same C_7 symmetry. In the case of $M113N_7$, βCD is bound with the secondary hydroxyl face "upward" (Fig. 2*B*). In each glucose unit of the βCD, the 2-hydroxyl is hydrogen bonded to the side-chain amide of an Asn-113 (the residue introduced by mutagenesis) and the

3-hydroxyl is hydrogen bonded to the ε-amino group of Lys-147. In the case of $M113F_7$, two βCDs are bound to the αHL pore (Fig. 2*C*). It is the top βCD in the structure that concerns us, because it is in contact with the Phe-113 residues introduced by mutagenesis. It is immediately apparent that the top βCD in $M113F_7$ is in the opposite orientation to the βCD in $M113N_7$ with each 6-hydroxyl group in a CH-π bonding interaction (31–35) with a Phe-113 side chain. The opposite orientations of the βCDs in $M113N_7$ and $M113F_7$ immediately explain why heteromers formed from similar numbers of M113N and M113F subunits (e.g., $M113N_4M113F_3$) bind βCD weakly (see also *Discussion*).

Unnatural Amino Acid Mutagenesis. To further explore the range of noncovalent interactions that are available when βCD binds to the αHL pore, five unnatural amino acids (Fig. 3*A* and Fig. S2) were incorporated at position 113, by using the in vitro nonsense codon suppression method (36). In particular, we had noted that $M113V_7$ containing the β-branched Val binds βCD tightly (15), and therefore we compared cyclopropylglycine (Cpg) and cyclopropylalanine (Cpa). We also further examined the means by which $M113F_7$ binds βCD tightly, by comparing the properties of 4-fluorophenylalanine (f1F), pentafluorophenylalanine (f5F), and cyclohexylalanine (Cha) at position 113.

The five homomeric pores all produced single-channel currents with unitary conductance values in the range expected for properly assembled heptamers (Fig. S3). All five bound βCD (Fig. 3*B, Level 2*), either tightly (f1F, Cpg) or weakly (f5F, Cha, Cpa) as described in detail below. During the long βCD binding events, additional current spikes were seen (Fig. 3*B*). Similar
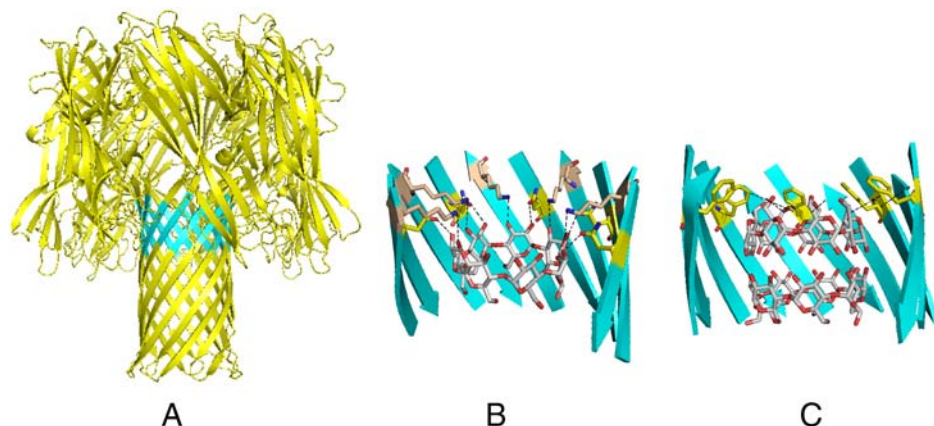
Fig. 2. X-ray structures of M113N and M113F homoheptamers with βCD bound. (*A*) Side view of heptameric αHL. βCD binds in the blue highlighted region. (*B*) βCD bound to M113N$_7$ (dotted lines indicate hydrogen bonding). The side chains of Lys-147 are in pale brown and the side chains of Asn-113 in yellow. (*C*) βCD bound to M113F$_7$ (dotted lines indicate CH-π bonding). The side chains of Phe-113 are in yellow. The second βCD in the M113F$_7 \cdot (\beta CD)_2$ structure is hydrogen bonded to the top βCD in a head-to-head arrangement and has no apparent interactions with the protein. For both (*B*) and (*C*), four β strands were omitted from the barrel to give a better view.

events had been observed previously with certain Met-113 replacement mutants and may represent movement of the βCD at its binding site (e.g., rotation about axes perpendicular to the C$_7$ axis) (15). The additional current spikes were more prevalent for M113V$_7$ and M113Cpg$_7$, which may take part in more conformationally labile interactions with βCD, compared with say M113F$_7$ (Fig. S4).

Interactions of βCD with Homoheptamers Bearing Aromatic Residues at Position 113. To further understand the nature of the binding of βCD to aromatic side chains, we examined the kinetics of βCD binding to the homoheptamers containing f1F or f5F at position 113, M113f1F$_7$ and M113f5F$_7$ (Fig. 3*C*). For both mutants, the value of k$_{on}$ was very similar to that of WT$_7$, but the values of k$_{off}$ and therefore K$_d$ for M113f1F$_7$ differed dramatically from WT$_7$ and were close to the values for the tight-binding mutant M113F$_7$ (Table S2*A*). By contrast, k$_{off}$ and K$_d$ for M113f5F$_7$ were similar to the values for WT$_7$ (Table S2*A*).

To determine whether M113f1F$_7$ binds βCD in the same orientation as M113F$_7$ (Fig. 2*C*), we made heteromers of the M113f1F subunit with M113N or M113F and examined M113F$_4$M113f1F$_3$ and M113N$_4$M113f1F$_3$. M113F$_4$M113f1F$_3$ binds βCD as strongly as either M113F$_7$ or M113f1F$_7$, but M113N$_4$M113f1F$_3$ binds βCD weakly with a similar affinity to WT$_7$ (Fig. 3*D* and Table S3). Therefore, it is reasonable to infer that M113F$_7$ and M113f1F$_7$ bind βCD in the same orientation with the 6-hydroxyl groups of the CD in proximity to the aromatic rings on the protein.

Cyclohexylalanine (Cha) was used to replace the aromatic side chains with a roughly isosteric hydrophobic group. Again the value of k$_{on}$ for βCD was little changed, but k$_{off}$ for M113Cha$_7$ had an intermediate value of 42 ± 6 s^{-1}. Therefore, M113Cha$_7$ binds βCD more weakly than M113F$_7$ but distinctly more strongly than the WT$_7$ pore (Table S2*A* and Fig. 3*C*).

Interactions of βCD with Homoheptamers Bearing Hydrophobic Residues at Position 113. M113V$_7$ binds βCD very strongly, and therefore we compared αHL pores with Cpg or Cpa at position 113. Cpg is roughly isosteric with Val, and like Val has a β-branched side chain. Gratifyingly, M113Cpg$_7$ has a k$_{on}$ value similar to the other αHL pores, and k$_{off}$ and K$_d$ values close to those of M113V$_7$ (Table S2*B* and Fig. 3*E*). Cyclopropylalanine (Cpa), with an additional methylene group compared to Cpg, is roughly isosteric with Leu, a weak binder, and M113Cpa$_7$ also binds βCD weakly with k$_{on}$, k$_{off}$ and K$_d$ values similar to those of WT$_7$ (Table S2*B* and Fig. 3*E*). M113I$_7$ and M113T$_7$, which are β-branched, are also weak binders, but Ile and Thr are less closely related to Val than Cpg.

To determine whether M113V$_7$ binds βCD in the same orientation as M113F$_7$ or M113N$_7$ (Fig. 2), we made heteromers of M113V and the M113N or M113F subunits. M113V$_3$M113F$_4$, M113V$_4$M113F$_3$, M113V$_3$M113N$_4$, and M113V$_4$M113N$_3$ were examined in detail. All four heteroheptamers bound βCD more weakly than M113V$_7$, M113F$_7$ or M113N$_7$ (Fig. 3*F* and Table S4), suggesting that Val at position 113 interacts with βCD strongly but in a different manner to either Phe or Asn. Each heteromer exhibited a range of K$_d$ values, perhaps reflecting the various possible permutations of the two different subunits around the central axis of the heptamer, although this heterogeneity was not seen for heteromers made from WT, M113F and M113N (Fig. 1).

Discussion

Soon after we discovered that βCD binds to the WT-αHL pore for around a millisecond, we found a mutant pore, M113N$_7$, that releases βCD ~10^4 times more slowly (14). This prompted us to examine all 19 mutants in which residue 113 is replaced by a natural amino acid, with the surprising result that a collection of amino acids with structurally unrelated side chains (V, H, Y, D, N, F) are tight binders (15). Here, we have examined the nature of the binding interactions more closely by single-channel electrical recording, protein engineering including unnatural amino acid mutagenesis, and high-resolution x-ray crystallography, and we provide the first definitive structural information on an engineered protein nanopore.

We find that βCD can bind tightly to the αHL pore in three different ways depending on the residue at 113, as exemplified by Asn, Phe, and Val. Because Asn and Phe have quite different side chains, we first compared the ability of M113N and M113F subunits to take part in binding the CD. The examination of heteromeric proteins containing WT (Met-113), M113N and M113F subunits showed that the replacement of WT subunits in WT$_7$ with M113N or M113F subunits led to increased affinity for βCD. The more M113N or M113F subunits that were added, the tighter binding became. By contrast, when subunits in M113N$_7$ were replaced with M113F subunits, binding became weaker, reaching a minimum at three to four M113F subunits, and then increasing in strength with five M113F subunits or more (Fig. 1*C*). Parallel structural studies (30) revealed the basis of the "opposing" effects of the M113N and M113F subunits. βCD binds to M113N$_7$ in the opposite orientation to that in which it binds to M113F$_7$. In M113N$_7$, the secondary hydroxyls in the βCD ring are hydrogen bonded to Lys-147 and Asn-113 (Fig. 2*A*). By contrast, βCD interacts with M113F$_7$ through its primary hydroxyl face (Fig. 2*B*).

It seemed likely that M113V$_7$, bound βCD in yet another way, and this was examined by forming heteromers between M113V and M113N or M113F. The presence of three or four subunits of either M113N or M113F greatly decreases the affinity of the pore for βCD (Fig. 3*F*), with an average k$_{off}$ of 7.3 × 10^1 s^{-1}, indicating that a third binding mode is indeed operating
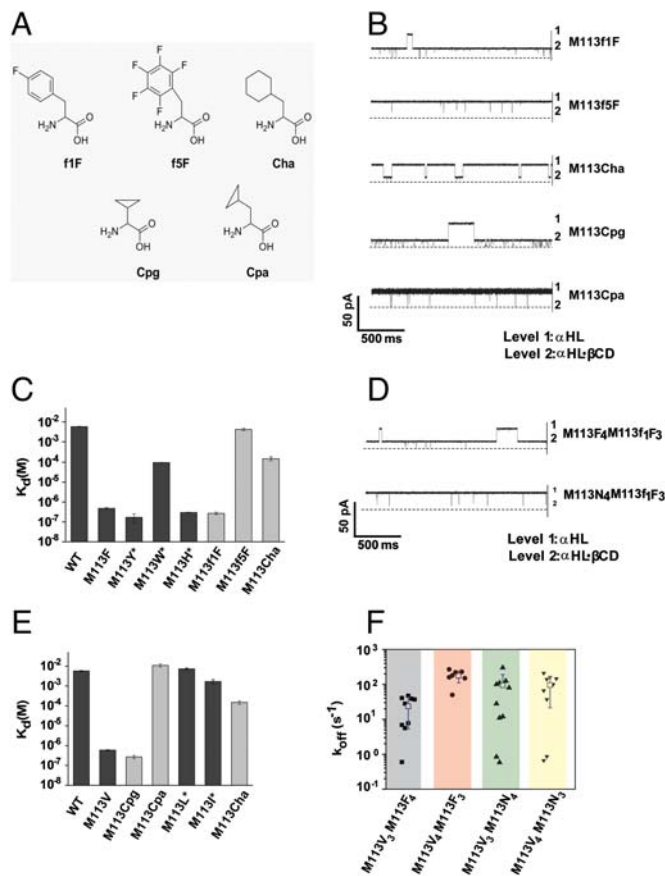
Fig. 3. Properties of pores containing natural and unnatural amino acid substitutions at position 113. The data were recorded at +40 mV in 1.0 M NaCl, 10 mM sodium phosphate, pH 7.5. (*A*) Unnatural amino acids used in this study: 4-fluorophenylalanine, f1F; pentafluorophenylalanine, f5F; cyclohexylalanine, Cha; cyclopropylglycine, Cpg; cyclopropylalanine, Cpa. (*B*) Representative current traces from single homoheptameric αHL pores, containing unnatural amino acids at position 113, in the presence of βCD. βCD (40 μM final) was added to the trans chamber. Level 1, open pore current; level 2, pore occupied by βCD. The broken line indicates zero current. (*C*) Interaction of βCD with homomeric αHL pores containing aromatic amino acids at position 113. K_d values for the interaction between βCD and the αHL pore were calculated by using $K_d = k_{off}/k_{on}$. Each column represents the mean ± s.d. for 10 or more determinations: dark gray, natural amino acids; light gray, unnatural amino acids. Data adapted from Gu and colleagues (15) are marked (*). (*D*) Representative current traces from single-channel recordings of βCD binding to M113F$_4$M113f1f$_3$ and M113N$_4$M113f1f$_3$. βCD (40 μM final) was added to the trans chamber. The broken line indicates zero current. (*E*) Interaction of βCD with homomeric αHL pores containing hydrophobic amino acids at position 113. K_d values for the interaction between βCD and the αHL pore were calculated by using $K_d = k_{off}/k_{on}$. Each column represents the mean ± s.d. for ten or more determinations: dark gray, natural amino acids; light gray, unnatural amino acids. Data adapted from Gu and colleagues (15) are marked (*). (*F*) k_{off} values for βCD from heteroheptamers formed with M113F and M113V subunits and with M113N and M113V subunits. βCD (40 μM final) was added to the trans chamber. The k_{on} values for βCD for all these mutants are similar, at $\sim3 \times 10^5$ M^{-1}s^{-1}. Empty square: average k_{off} values for the mutant (bar is ±s.d). Filled square: M113V$_3$M113F$_4$; filled circle: M113V$_4$M113F$_3$; filled upright triangle: M113V$_3$M113N$_4$; filled inverted triangle: M113V$_4$M113N$_3$.

(Table S4). In summary, the three groups of tight-binding mutants comprise αHL pores incorporating, at position 113: (*i*) the hydrogen-bonding amino acids N, D (the latter would have to be largely in the protonated form), and possibly H; (*ii*) the aromatics F, Y, f1F, and possibly H, and more weakly W; (*iii*) the β-branched amino acids V, Cpg. There may be yet other means by which CDs can bind to the αHL pore. For example, we earlier found that hepta-6-sulfato-βCD can bind tightly to αHL pores containing the

N139Q mutation (37). Presumably, this CD is bound at a site lower down in the β barrel in a fashion that includes hydrogen bonding to the Gln at position 139. While the various mutants exhibited widely different k_{off} values, the value of k_{on} was almost invariant and averaged $\sim2.3 \times 10^5$ M^{-1}s^{-1} (Table S2) (15). Apparently, transport to the binding site is rate limiting, through a route unaffected by mutagenesis.

k_{off} increased precipitously with the addition of WT subunits to M113N$_7$ (Fig. 1*C*). Crystal structures of M113N$_7$ show that residues 111, 113, and 147 are reorganized by comparison with WT$_7$ and then undergo a more limited rearrangement when βCD binds (Fig. S5). For example, the side chain of Lys-147 shifts position to form a bifurcated hydrogen bond with a 3-hydroxyl group of βCD and the side chain carbonyl of an Asn-113 (Fig. S6). Therefore, the side chains of residues 111, 113, and 147 might be in a variety of conformations in WT$_{7-n}$M113N$_n$ heteromers and offer less well preorganized binding sites for βCD than they do in M113N$_7$. Further, the intramolecular hydrogen bonds of the secondary hydroxyls in βCD (38) must be disrupted upon binding as both hydroxyls on each glucose ring form hydrogen bonds to the mutant subunits (Fig. 2*B*). Because the hydrogen bonds that are broken in βCD are arranged in a circle, the breakage of bonds involving a single glucose (three bonds in all) will be relatively more disruptive than those involving adjoining glucose residues or the entire circle. The overall binding cooperativity in M113N$_7$ could be attributed to enthalpic cooperativity outweighing entropic penalties to binding (39). Positive cooperativity has been observed previously in fairly rigid model systems (40).

By contrast with M113N$_7$, there is little movement of side chains in (M113F)$_7$ by comparison with WT$_7$ and little movement, including Phe-113, upon binding βCD (Fig. S7*A*). Further, the crystal structure of M113F$_7$ · βCD suggests that each Phe residue interacts independently with the βCD through what appear to be CH-π interactions (Fig. S7*B*). These interactions are expected to be weak and not strongly directional and hence offer less enthalpic cooperativity, as supported by the B-factors (crystallographic temperatures factors) at the primary βCD binding site, which are between ~40 and 50. Positive cooperativity is observed, but it is less pronounced than in the case of M113N$_7$ (Table S5). In the case of M113N$_7$, the B-factors of the residues that bind βCD are in the 20s implying that the βCD is more rigidly held than it is in M113F$_7$.

The binding of sugars to aromatic residues in proteins can include CH-π bonding (41) or OH-π bonding or a finely balanced complement of both (42, 43). However, we have dismissed the possibility of an OH-π interaction between Phe-113 and the 6-hydroxyl groups of βCD as the distance between the center of the phenyl rings to the nearest hydroxyl oxygen is higher (5.2 ± 0.65 Å, $n = 7$) than that expected for a favorable OH-π interaction (33). While we propose that βCD binds to Phe-113 through a C-6 CH-π interaction (Fig. S7*B*), the distances between the center of the Phe-113 ring and the nearest C-6 of βCD observed in the M113F$_7$ · βCD structure (4.66 ± 0.24 Å, $n = 7$) are in the upper range of the expected distance for a strong interaction, which is ~4.5 Å (33). The angle between the normal to the aromatic rings and the line connecting the C-6 atoms to the aromatic midpoint is $8.0 \pm 5.6°$, which is well within the expected range (44). The measurements with M113f5F$_7$ argue against a hydrophobic interaction between Phe residues at position 113 and the βCD ring. In f5F, the hydrophobicity of the phenyl ring is significantly increased (45) yet M113f5F$_7$ binds βCD weakly, like WT$_7$ (Fig. 3*C* and Table S2*A*).

By contrast with F, f1F, Y and N, homomeric αHL pores with f5F and W at position 113 bound βCD relatively weakly (Fig. 3*C* and Table S2*A*). In the case of f5F, the powerful electron withdrawing action of the five fluorine atoms leaves a highly increased positive charge at the center of the ring (46, 47), mitigating against a hydrogen-bonding interaction. The electron-rich Trp
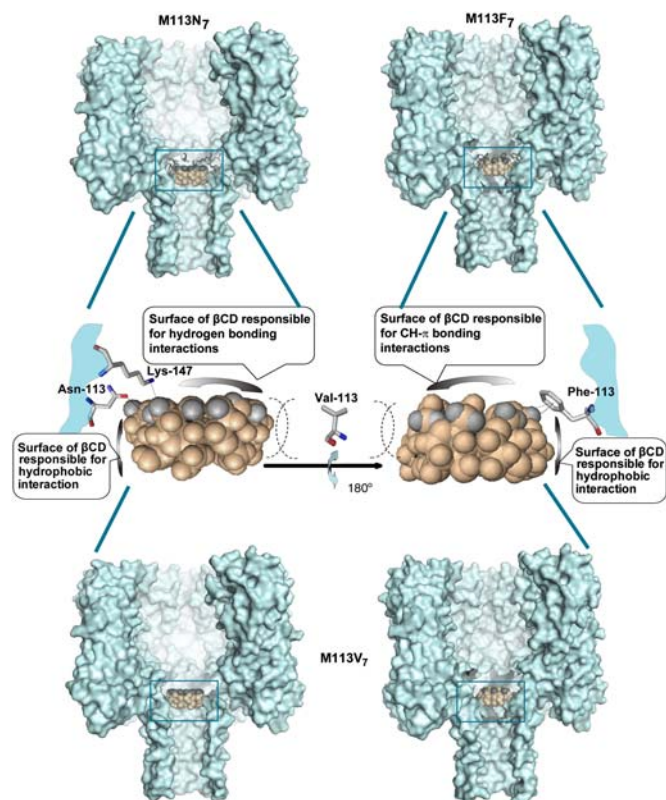
Fig. 4. Molecular model showing the three classes of interaction between the αHL pore and βCD identified in this work. The model identifies the region of βCD responsible for each interaction (H atoms interacting with Phe-113 or Asn-113 and Lys-147: gray). The first class of interaction is with aromatic residues and involves the seven -CH$_2$OH groups of the βCD. The second class is typified by the interactions with Asn at position 113, which involve hydrogen-bonds to the secondary 2-hydroxyls of the βCD. Structural studies show that this interaction is supported by hydrogen bonding between Lys-147 and the secondary 3-hydroxyls of the βCD. Structural studies and experiments with heteromers suggest that the βCD in M113F$_7$ is in the opposite orientation to the βCD in M113N$_7$, in support of the model shown here. As the interaction with Val is hydrophobic, it is not directional and βCD may not bind at the same position inside the β barrel as it does in M113F$_7$ or M113N$_7$.

ring (44, 46, 47) should favor hydrogen bonding, but here we cannot make a direct comparison with the crystal structure of M113F$_7$ as the indole ring is far larger than benzene. It is possible that it cannot become oriented in the same manner and that it is misaligned for hydrogen bonding.

Our experiments suggest that M113V$_7$ and M113Cpg$_7$ bind βCD in a third way. In heteromers with M113V, both M113F and M113N reduce the affinity of the pore for βCD suggesting that neither the CH-π interaction with Phe-113 nor the hydrogen-bonding interactions with Asn-113 and Lys-147 are compatible with binding to Val. Close interactions of Val with glucose rings have been noted previously (48). Therefore, we propose that the Val side-chain interacts with the side of the glucose ring. This interaction might occur in one or both orientations of the CD ring (Fig. 4).

Conclusion

We provide structural information on engineered protein nanopores and describe three distinct ways in which βCD can bind within the lumen of mutant αHL pores in atomic detail. Our results will be useful in several areas of basic science and biotechnology. By using host molecules lodged within the αHL pore, host-guest interactions can be investigated in fine detail at the single-molecule level (17, 49). The present work will now permit us to examine binding events at a known face of a CD. The work

also provides information for designing new binding sites within the lumen of the αHL pore (37) or within other β barrel proteins (21, 50) and for using molecular design to devise ways in which to covalently attach CDs within pores (13, 51). These areas impact practical applications of nanopore technology including stochastic sensing (8), single-molecule DNA sequencing (9, 12, 13, 52), the use of nanoreactors for the observation of single-molecule chemistry (10), and the construction of nano- and microdevices (11, 53), as well as the design of CDs as therapeutic agents (23, 24).

Methods

Full details of the experimental procedures can be found in *SI Appendix*.

Materials

L-Amino acids were obtained as follows: 4-fluorophenylalanine (f1F) (Fluka); pentafluorophenylalanine (f5F) (PepTech Corp.); cyclopropylglycine (Cpg) (Tyger); cyclopropylalanine (Cpa) (Tyger). 4-*N*-benzoyl-5′-*O*-(4,4′-dimethoxytrityl)-2′-deoxycytidine-3′-[(2-cyanoethyl)-(*N,N*-diisopropyl)]-phosphoramidite and bis(2-cyanoethyl)-*N,N*-diisopropylphosphoramidite for the synthesis of pdCpA were purchased from Glen Research and Toronto Research Chemicals, respectively.

Preparation of NVOC-Protected Aminoacyl-pdCpA. NVOC-protected aminoacyl-pdCpAs were prepared as reported previously by reacting the dinucleotide pdCpA with N-protected, carboxylic acid-activated, amino acids (54–56).

Preparation of NVOC-Protected Aminoacyl-tRNA. NVOC-protected aminoacyl-pdCpAs were ligated enzymatically with a truncated tRNA, prepared by using methods described elsewhere (57, 58).

Genetic Constructs and Mutagenesis. All new αHL constructs were verified by DNA sequencing. Details of each construct can be found in *SI Appendix*.

Synthesis, Assembly, and Purification of Mutant αHL pores. αHL monomers (WT and mutants) were prepared in vitro by coupled transcription and translation (IVTT) and assembled into homoheptamers on rabbit red blood cell membranes followed by purification by SDS–PAGE as described earlier (59). Heteroheptamers were prepared by mixing the two required DNAs (one encoding an αHL with a D8 tail) before IVTT and then oligomerizing the mixed translation products on rabbit red blood cell membranes. Pores with the desired combinations of subunits were purified by SDS–PAGE (59).

Synthesis, Assembly, and Purification of αHL Mutants Containing Unnatural Amino Acids. αHL polypeptides containing unnatural amino acids were synthesized by IVTT in the presence of rabbit red blood cell membranes. The plasmid with a stop codon (TAG) at position 113 was used. Deprotected aminoacyl-tRNAs (*SI Appendix*) were added to the IVTT mixtures. For heteroheptamers with subunits containing unnatural amino acids in combination with M113N or M113F, monomers were first made, which were then coassembled on rabbit red blood cell membranes and subsequently purified by SDS–PAGE.

Single-Channel Current Recordings in Planar Lipid Bilayers. (15, 60) Recordings were made with 1.0 M NaCl, 10 mM sodium phosphate, pH 7.5, in both chambers, at an applied potential of +40 mV. Data were recorded at 22 ± 2°C. The bilayer was formed from 1,2-diphytanoyl-*sn*-glycero-phosphocholine (Avanti Polar Lipids). Proteins were added to the cis chamber, and βCD to the trans chamber. Single-channel currents were recorded with an Axopatch 200B patch-clamp amplifier (Axon Instruments) and filtered at 2 kHz with a built-in 4-pole low-pass Bessel Filter. The data were acquired at a sampling rate of 10 kHz. For mutants that bind βCD strongly, the data were acquired for at least 30 min and for weak-binding mutants for at least 10 min.

Kinetic Data Analysis. Current amplitude and dwell-time histograms were made by using ClampFit 9.0. The mean dwell times, τ_{off}, were determined by fitting the dwell-time histograms to single exponentials. Values of k_{on} and k_{off} were obtained by using the mean dwell times and mean interevent intervals, as described previously (15, 60). This analysis assumes a binary interaction, which was supported in all cases examined by the finding of only one major blockade level and a single exponential distribution of dwell times (τ_{off}).

BIOCHEMISTRY

1. Lu Y, Yeung N, Sieracki N, Marshall NM (2009) Design of functional metalloproteins. *Nature* 460:855–862.
2. Gebauer M, Skerra A (2009) Engineered protein scaffolds as next-generation antibody therapeutics. *Curr Opin Chem Biol* 13:245–255.
3. Gronwall C, Stahl S (2009) Engineered affinity proteins—Generation and applications. *J Biotechnol* 140:254–269.
4. Arnold U (2009) Incorporation of non-natural modules into proteins: Structural features beyond the genetic code. *Biotechnol Lett* 31:1129–1139.
5. Tracewell CA, Arnold FH (2009) Directed enzyme evolution: Climbing fitness peaks one amino acid at a time. *Curr Opin Chem Biol* 13:3–9.
6. Fruk L, Kuo CH, Torres E, Niemeyer CM (2009) Apoenzyme reconstitution as a chemical tool for structural enzymology and biotechnology. *Angew Chem Int Ed Engl* 48:1550–1574.
7. Bayley H, Jayasinghe L (2004) Functional engineered channels and pores. *Mol Membr Biol* 21:209–220.
8. Bayley H, Cremer PS (2001) Stochastic sensors inspired by biology. *Nature* 413:226–230.
9. Branton D, et al. (2008) The potential and challenges of nanopore sequencing. *Nature Biotechnol* 26:1146–1153.
10. Bayley H, Luchian T, Shin S-H, Steffensen MB (2008) *Single Molecules and Nanotechnology*, eds R Rigler and H Vogel (Springer, Heidelberg), pp 251–277.
11. Maglia G, et al. (2009) Droplet networks with incorporated protein diodes show collective properties. *Nat Nanotechnol* 4:437–440.
12. Astier Y, Braha O, Bayley H (2006) Toward single molecule DNA sequencing: Direct identification of ribonucleoside and deoxyribonucleoside 5'-monophosphates by using an engineered protein nanopore equipped with a molecular adapter. *J Am Chem Soc* 128:1705–1710.
13. Clarke J, et al. (2009) Continuous base identification for single-molecule nanopore DNA sequencing. *Nature Nanotechnol* 4:265–270.
14. Gu L-Q, Braha O, Conlan S, Cheley S, Bayley H (1999) Stochastic sensing of organic analytes by a pore-forming protein containing a molecular adapter. *Nature* 398:686–690.
15. Gu L-Q, Cheley S, Bayley H (2001) Prolonged residence time of a noncovalent molecular adapter, β-cyclodextrin, within the lumen of mutant α-hemolysin pores. *J Gen Physiol* 118:481–494.
16. Ervin EN, Kawano R, White RJ, White HS (2008) Simultaneous alternating and direct current readout of protein ion channel blocking events using glass nanopore membranes. *Anal Chem* 80:2069–2076.
17. Gurnev PA, Harries D, Parsegian VA, Bezrukov SM (2009) The dynamic side of the Hofmeister effect: A single-molecule nanopore study of specific complex formation. *ChemPhysChem* 10:1445–1449.
18. Mamonova T, Kurnikova M (2006) Structure and energetics of channel-forming protein-polysaccharide complexes inferred via computational statistical thermodynamics. *J Phys Chem B* 110:25091–25100.
19. Egwolf B, Luo Y, Walters DE, Roux B (2010) Ion selectivity of alpha-hemolysin with beta-cyclodextrin adapter. II. Multi-ion effects studied with grand canonical monte carlo/brownian dynamics simulations. *J Phys Chem B* 114:2901–2909.
20. Orlik F, et al. (2003) CymA of Klebsiella oxytoca outer membrane: Binding of cyclodextrins and study of the current noise of the open membrane. *Biophys J* 85:876–885.
21. Chen M, Khalid S, Sansom MSP, Bayley H (2008) OmpG: Engineering a quiet pore for biosensing. *Proc Natl Acad Sci USA* 105:6272–6277.
22. Locke D, Koreen IV, Liu JY, Harris AL (2004) Reversible pore block of connexin channels by cyclodextrins. *J Biol Chem* 279:22883–22892.
23. Karginov VA, Nestorovich EM, Moayeri M, Leppla SH, Bezrukov SM (2005) Blocking anthrax lethal toxin at the protective antigen channel by using structure-inspired drug design. *Proc Natl Acad Sci USA* 102:15075–15080.
24. Moayeri M, Robinson TM, Leppla SH, Karginov VA (2008) In vivo efficacy of beta-cyclodextrin derivatives against anthrax lethal toxin. *Antimicrob Agents Chemother* 52:2239–2241.
25. Gao C, Ding S, Tan Q, Gu LQ (2009) Method of creating a nanopore-terminated probe for single-molecule enantiomer discrimination. *Anal Chem* 81:80–86.
26. Pregel MJ, Jullien L, Lehn J-M (1992) Towards artificial ion channels: Transport of alkali metal ions across liposomal membranes by "bouquet" molecules. *Angew Chem Int Edit* 31:1637–1639.
27. Bacri L, Benkhaled A, Guegan P, Auvray L (2005) Ionic channel behavior of modified cyclodextrins inserted in lipid membranes. *Langmuir* 21:5842–5846.
28. Jog PV, Gin MS (2008) A light-gated synthetic ion channel. *Org Lett* 10:3693–3696.
29. Howorka S, Cheley S, Bayley H (2001) Sequence-specific detection of individual DNA strands using engineered nanopores. *Nat Biotechnol* 19:636–639.
30. Montoya M (2004) *Insights into Membrane Association and Bioengineering of a Pore-Forming Toxin: Structural Studies of Staphylococcal α-Hemolysin* (Columbia University, New York).
31. Steiner T (2002) The hydrogen bond in the solid state. *Angew Chem Int Ed* 41:49–76.
32. Steiner T (2002) Hydrogen bonds from water molecules to aromatic acceptors in very high-resolution protein crystal structures. *Biophys Chem* 95:195–201.
33. Steiner T, Koellner G (2001) Hydrogen bonds with pi-acceptors in proteins: Frequencies and role in stabilizing local 3D structures. *J Mol Biol* 305:535–557.
34. Brandl M, Weiss MS, Jabs A, Sühnel J, Hilgenfeld R (2001) CH...π-interactions in proteins. *J Mol Biol* 307:357–377.
35. Weiss MS, Brandl M, Suhnel J, Pal D, Hilgenfeld R (2001) More hydrogen bonds for the (structural) biologist. *Trends Biochem Sci* 26:521–523.
36. Wang L, Xie J, Schultz PG (2006) Expanding the genetic code. *Annu Rev Biophys Biomol Struct* 35:225–249.
37. Gu L-Q, Cheley S, Bayley H (2001) Capture of a single molecule in a nanocavity. *Science* 291:636–640.
38. Saenger W, et al. (1998) Structures of the common cyclodextrins and their larger analogues—Beyond the doughnut. *Chem Rev* 98:1787–1802.
39. Hunter CA, Tomas S (2003) Cooperativity, partially bound states, and enthalpy-entropy compensation. *Chem Biol* 10:1023–1032.
40. Bisson AP, Hunter CA (1996) Cooperativity in the assembly of zipper complexes. *Chem Commun* 1723–1724.
41. del Carmen Fernandez-Alonso M, Canada FJ, Jimenez-Barbero J, Cuevas G (2005) Molecular recognition of saccharides by proteins. Insights on the origin of the carbohydrate-aromatic interactions. *J Am Chem Soc* 127:7379–7386.
42. Jimenez-Barbero J, Asensio JL, Canada FJ, Poveda A (1999) Free and protein-bound carbohydrate structures. *Curr Opin Struct Biol* 9:549–555.
43. Stanca-Kaposta EC, et al. (2007) Carbohydrate molecular recognition: A spectroscopic investigation of carbohydrate-aromatic interactions. *Phys Chem Chem Phys* 9:4444–4451.
44. Brandl M, Weiss MS, Jabs A, Suhnel J, Hilgenfeld R (2001) CH...π-interactions in proteins. *J Mol Biol* 307:357–377.
45. Woll MG, Hadley EB, Mecozzi S, Gellman SH (2006) Stabilizing and destabilizing effects of phenylalanine -->F5-phenylalanine mutations on the folding of a small protein. *J Am Chem Soc* 128:15932–15933.
46. Mecozzi S, West AP, Jr, Dougherty DA (1996) Cation-pi interactions in aromatics of biological and medicinal interest: Electrostatic potential surfaces as a useful qualitative guide. *Proc Natl Acad Sci USA* 93:10566–10571.
47. Dougherty DA (2008) Cys-loop neuroreceptors: Structure to the rescue?. *Chem Rev* 108:1642–1653.
48. Hondoh H, et al. (2008) Substrate recognition mechanism of alpha-1,6-glucosidic linkage hydrolyzing enzyme, dextran glucosidase from Streptococcus mutans. *J Mol Biol* 378:913–922.
49. Kang XF, Cheley S, Guan X, Bayley H (2006) Stochastic detection of enantiomers. *J Am Chem Soc* 128:10684–10685.
50. Chen M, Li QH, Bayley H (2008) Orientation of the monomeric porin OmpG in planar lipid bilayers. *ChemBioChem* 9:3029–3036.
51. Wu H-C, Astier Y, Maglia G, Mikhailova E, Bayley H (2007) Protein nanopores with covalently attached molecular adapters. *J Am Chem Soc* 129:16142–16148.
52. Bayley H (2006) Sequencing single molecules of DNA. *Curr Opin Chem Biol* 10:628–637.
53. Astier Y, Bayley H, Howorka S (2005) Protein components for nanodevices. *Curr Opin Chem Biol* 9:576–584.
54. Robertson SA, Noren CJ, Anthony-Cahill SJ, Griffith MC, Schultz PG (1989) The use of 5'-phospho-2 deoxyribocytidylylriboadenosine as a facile route to chemical aminoacylation of tRNA. *Nucleic Acids Res* 17:9649–9660.
55. Ellman J, Mendel D, Anthony-Cahill S, Noren CJ, Schultz PG (1991) Biosynthetic method for introducing unnatural amino acids site-specifically into proteins. *Method Enzymol* 202:301–336.
56. Kearney PC, et al. (1996) Dose-response relations for unnatural amino acids at the agonist binding site of the nicotinic acetylcholine receptor: Tests with novel side chains and with several agonists. *Mol Pharmacol* 50:1401–1412.
57. England TE, Bruce AG, Uhlenbeck OC (1980) Specific labeling of 3′ termini of RNA with T4 RNA ligase. *Method Enzymol* 65:65–74.
58. Nowak MW, et al. (1998) In vivo incorporation of unnatural amino acids into ion channels in xenopus oocyte expression system. *Method Enzymol* 293:504–529.
59. Cheley S, Braha O, Lu X, Conlan S, Bayley H (1999) A functional protein pore with a "retro" transmembrane domain. *Protein Sci* 8:1257–1267.
60. Gu L-Q, et al. (2000) Reversal of charge selectivity in transmembrane protein pores by using non-covalent molecular adapters. *Proc Natl Acad Sci USA* 97:3959–3964.
61. Song L, et al. (1996) Structure of staphylococcal α-hemolysin, a heptameric transmembrane pore. *Science* 274:1859–1865.